Single-carrier 72 GBaud 32QAM and 84 GBaud 16QAM transmission using a SiP IQ modulator with joint digital-optical pre-compensation

Jiachuan Lin, Hassan Sepehrian, Leslie A. Rusch, and Wei Shi

OSA Optics Express, (Volume 27, Issue 4) (2019)

https://doi.org/10.1364/OE.27.005610

Single-carrier 72 GBaud 32QAM and 84 GBaud 16QAM transmission using a SiP IQ modulator with joint digital-optical pre-compensation

JIACHUAN LIN,[1] HASSAN SEPEHRIAN,[1] LESLIE A. RUSCH,[1] AND WEI SHI[1,*]

[1] *Department of Electrical and Computer Engineering, Center for Optics, Photonics and Lasers (COPL), Université Laval, Québec, Canada*
[*] *wei.shi@gel.ulaval.ca*

Abstract: We establish experimentally the suitability of an all-silicon optical modulator to support future ultra-high-capacity coherent optical transmission links beyond 400 Gb/s. We present single-carrier data transmission from 400 Gb/s to 600 Gb/s using an all-silicon IQ modulator produced with a generic foundry process. The operating point of the silicon photonic transmitter is carefully optimized to find the best efficiency bandwidth trade-off. We present a methodology to split pre-compensation between digital and optical stages. For the 400 Gb/s transmission, we achieved 60 Gbaud dual-polarization (DP)-16QAM, reaching a distance of 1,520 km. Transmission of 500 Gb/s was further tested using 75 Gbaud 16QAM and 60 Gbaud 32QAM, reaching 1,120 km and 480 km, respectively. We finally demonstrated 72 Gbaud DP-32QAM (720 Gb/s) transmitted over 160 km and 84 Gbaud DP-16QAM (672 Gb/s) transmitted over 720 km, meeting the threshold for 20% forward error correction overhead and achieving net rates of 600 Gb/s and 576 Gb/s, respectively. To the best of our knowledge, these are the highest baud-rate coherent transmission results achieved using an all-silicon IQ modulator. We have demonstrated that we can reap the myriad advantages of SiP integration for transmission at extreme bit rates.

1. Introduction

The exponential growth of global data traffic to meet the demand of cloud computing, mobile Internet, Internet of things, and artificial intelligence, drives optical networks towards a single line rate of 400G-1Tb and beyond. Recently, single carrier transmissions with data rates from 400G to 1Tb have been demonstrated either using electrical time domain multiplexing (ETDM) or a single digital-to-analog converter (DAC) [1–3]. In [3], a record rate of single carrier 1 Tb/s transmission was demonstrated by 100 Gbaud 64QAM (quadrature amplitude modulation) using a single $LiNbO_3$ modulator and a BiCMOS DAC. However, it is challenging to further scale optical transceivers based on $LiNbO_3$ without undue system complexity in the face of platform constraints.

In contrast, photonic integrated circuits can be easily scaled and are considered key enablers of future wavelength division multiplexing (WDM) systems [4]. Using densely integrated high bandwidth optical transceivers, the footprint and power consumption of WDM systems will be dramatically reduced compared to current solutions using bulky discrete optical components. High-baud-rate, single-carrier transmission has also been extensively explored on photonic integration platforms, such as InP for 100 Gbaud 32QAM [5], 77 Gbaud 32QAM [6] and 120 Gbaud QPSK (quaternary phase shift keying) [7], thin film polymer on silicon for 90 Gbaud QPSK [8] and organic hybrid for 100 Gbaud 16QAM [9].

Compared to other integration platforms, silicon photonics (SiP) leverages the mature complementary metal-oxide-semiconductor (CMOS) technology and offers a smaller form factor,

National Science and Engineering Research Council of Canada (NSERC) Funding: CRDPJ 486716-15

for lower-cost mass production and ultra-large-scale photonic integration [10, 11]. All-silicon modulators are preferred as they are readily integrated with other photonic components on the same fabrication process.

In [12], 56 Gbaud QPSK was demonstrated with an on-chip equalizer. In [13], 30 Gbaud 64QAM was generated with digital pre-compensations using a high-speed digital-to-analog converter (DAC). In [14], dual-polarization emulated 455 Gb/s orthogonal frequency division multiplexed (OFDM) transmission was demonstrated, which, however, required high overhead (47%) forward error correction (FEC), resulting in a net bit rate less than 300 Gb/s. The same work also reported 42 Gbaud Nyquist-16QAM transmission. In [15], 96 Gbaud on-off keying and 28 Gbaud QPSK are demonstrated. All these demonstrations have net data rates below 400 Gb/s, lower than rates reported for $LiNbO_3$ or hybrid integrated counterparts. Single-carrier, higher-order QAM with net bit rates above 400 Gb/s in an all-silicon modulator has yet to be reported.

In this paper, we examine high-baud-rate QAM transmission using a silicon traveling-wave (TW) IQ (in phase/quadrature) modulator optimized based on a CMOS-compatible large-wafer photonics fabrication process. We demonstrate a joint optimization procedure of optical and digital pre-emphasis filters for the silicon coherent transmitter. While the combination of the electrical and optical equalization has been previously used in coherent transmission, the digital and optical filters were conventionally treated independently. In [3], the applied digital pre-compensation filter is obtained by calibrating an electrical B2B system, then an optical filter is applied to take care of the remaining frequency slope. However, this digital-first method does not explore the overall joint E/O optimization. In [1], the authors studied the joint optimization of optical pre-compensation filter and post-digital filter in an ETDM 120 Gbaud system. Their results show that such a joint optimization approach can help achieve better performance. However, due to the DAC-less operation, digital pre-compensation was not taken into consideration. In this paper, we show a thorough procedure to optimize the split of pre-compensation between digital and optical domains for different baud rates. The results show that, a joint optimization on digital and optical pre-compensation filters help mitigate signal degradation for a bandwidth severely limited silicon transmitter. Up to 72 Gbaud DP-32QAM and 84 Gbaud dual-polarization (DP)-16QAM are successfully generated and detected in a back-to-back (B2B) configuration and over distance in a standard single mode fiber (SSMF) and EDFA link. In addition, 60 Gbaud DP-16QAM are also tested, targeting single-carrier 400G, and 75G Gbaud 16QAM and 60 Gbaud DP-32QAM are for 500G implementations.

The rest of the paper is organized as follows. Section 2 describes the design and electro-optical (E/O) properties of our SiP IQ modulator. Section 3 details our experimental setup for single carrier transmission, including the SiP test platform, high baud rate QAM generation, coherent detection, and applied digital signal processing (DSP). Section 4 discusses the optimizations of digital and optical pre-compensation filters used for high baud rate implementation. In section 5, we show and discuss the results of B2B BER vs. OSNR performance, and distance transmission. Finally, we offer some concluding remarks in section 6.

2. Silicon photonics IQ modulator design and characterization

The schematic of our silicon IQ modulator design is shown in Fig. 1. It consists of two Mach-Zehnder modulators (MZMs) applying TW electrodes. A laterally doped p-n junction in a 220-nm-high silicon rib waveguide is used as the phase shifter (Fig. 1(b)). Three levels of dopants are applied to reduce the junction resistance without introducing excess optical loss. The device was fabricated using a CMOS-compatible process (A∗IME, Singapore) with 193-nm lithography. The MZM uses a series push-pull driving configuration, which imposes lower capacitive load for higher bandwidth compared to the dual-drive configuration [16]. Each TW-MZM uses a coplanar stripline (CPS) transmission line with on-chip 50 Ω termination implemented using

National Science and Engineering Research Council of Canada (NSERC) Funding: CRDPJ 486716-15

semiconductor resistors. We use T-shaped extensions to satisfy the velocity and impedance matching requirements simultaneously (Fig. 1(b)). A longer phase shifter can reduce the driving voltage but leads to lower bandwidth due to the high RF loss in the p-n junction. We chose a length of 4.5 mm for this trade-off. More details of the modulator design can be found in [17].

The two TW-MZMs are placed 700 μm apart to prevent excitation of unwanted RF modes (slot modes) in the TW electrodes [18], and to decrease electro-optic interference. Metal heaters are used to introduce a $\pi/2$ phase shift between the I and Q branches and to balance the two arms of each MZM. On-chip insertion loss of the IQ modulator is measured to be 6.8 dB. The coupling loss from a fiber array to the I/O grating couplers on the SiP die was 8.5 dB. Due to fabrication imperfections, the two TW-MZMs have slightly different V_π.

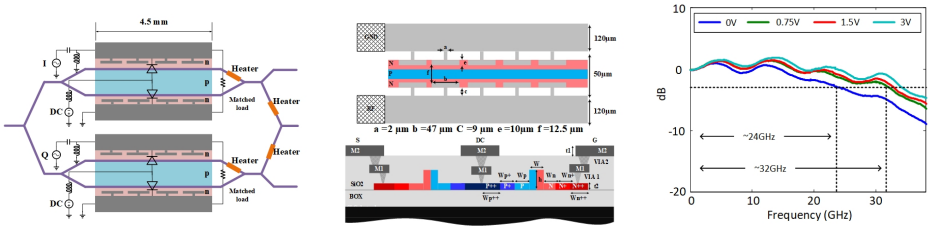

(a) (b) (c)

Fig. 1. (a) SiP IQ modulator employing TW-MZM in a series push-pull driving configuration, (b) top view of the slow-wave electrode (upper schematic) and cross section of the lateral P-N junction waveguide (lower schematic): Wp++= 5.2, Wp+= 0.83, Wp= 0.37, Wn++= 5.2, Wn+= 0.81, Wn= 0.39, W=0.5, h=0.22, t1=2, t2=0.9 (all dimensions are in μm), and (c) E-O frequency response of the SiP TW-MZMs averaged over IQ branches for several reverse bias voltages.

The frequency response of the modulator is estimated by measuring and fitting the optical spectrum for modulation with a digitally pre-equalized 80-Gbaud Nyquist-16QAM training sequence with a roll-off factor of 0.01. For the purpose of calibration, we first measure the overall frequency response of the driving setup (consisting of components such as the DAC, RF drivers and cables) in a B2B configuration using a 60-GHz real-time oscilloscope (RTO). The frequency response of the setup is then de-embedded from the driving signal by applying a minimum mean square error (MMSE) filter to obtain a flat RF spectrum fed to the modulator. The optical spectrum after modulation is then captured using a high-resolution optical spectrum analyzer (OSA), which represents the frequency response of the RF-probed silicon modulator. Figure 1(c) shows the measured frequency response at different reverse biases. The estimated 3 dB bandwidth is ~24 GHz at zero bias, ~32 GHz at 0.75 V and ~34 GHz at 3 V. These results show good agreement with that obtained using a 67-GHz vector network analyzer in our lab. The ripples of the frequency response are caused by the imperfect RF impedance matching in the modulator (i.e., the TW electrode loaded by the pn-junctions) and RF probing, which can be suppressed using digital pre-compensation. Notice that a 50-GHz RF probe is used in the test, whose response is not excluded here; thus, the real performance of the modulator should be slightly better than the results shown in Fig. 1(c).

3. Single carrier transmission test platform

The testbed configuration of the SiP IQ modulator single carrier transmission is shown in Fig. 2. A continuous wave carrier at 1530 nm with 100 kHz linewidth is provided by an external cavity laser (ECL). The carrier is boosted to 23 dBm by a high power erbium doped fiber amplifier (EDFA), and then coupled into the silicon chip through a fiber array. The data modulation is

National Science and Engineering Research Council of Canada (NSERC) Funding: CRDPJ 486716-15

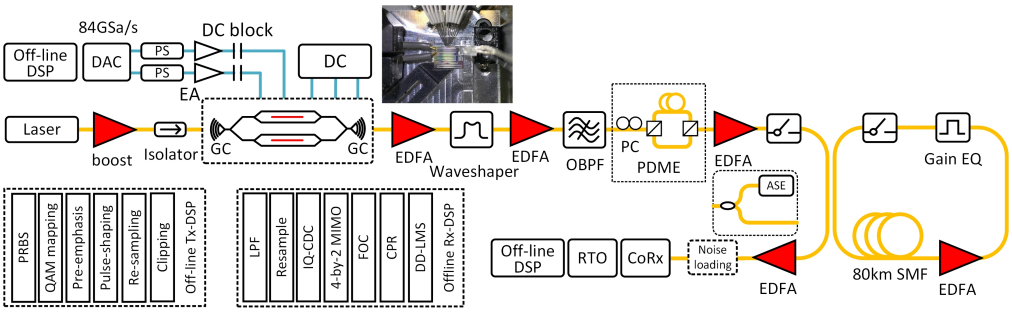

Fig. 2. Experimental setup of SiP IQ modulator single carrier transmission. DSP: digital signal processing; DAC: digital-to-analog converter; PS: phase shifter; GC: grating coupler; OBPF: optical bandpass filter; PC: polarization controller; PDME: polarization division multiplexing emulator; SMF: single mode fiber; CoRx: coherent receiver; LPF: low pass filter; CDC: chromatic dispersion compensation; MIMO: multi-inputs-multi-outputs; FOC: frequency offset compensation; CPR: carrier phase recovery; DD-LMS: decision directed least mean square filter.

realized by probing the silicon IQ modulator with digitally pulse-shaped I and Q driving signals generated by an 8-bit DAC operating at 84 GSa/s. The digital pulse shaping is processed off-line as illustrated in the transmitter-end (Tx) digital signal processing flowchart insert in Fig. 2. A pseudo random binary sequence (PRBS) of order 19 is mapped to Grey-coded QAM symbols, and then a pre-measured one-sample per symbol (SPS) precompensation filter is applied. After precompensation, the QAM symbols are raised-cosine shaped, with roll-off factor of 0.01, to achieve a time domain Nyquist pulse. The pulse-shaped samples are re-sampled to match the DAC sampling rate for various signal baud rates ranging from 60 Gbaud to 84 Gbaud. After clipping and quantization, these samples are loaded to the DAC. The outputs of the DAC are amplified by 50 GHz 18 dBm RF drivers. The I and Q signals are carefully de-skewed by tuning a pair of RF phase shifters. The driving signals are applied to the modulator through a GS-SG configured probe.

For QAM modulation, the MZMs of the two arms are operated at their null points by appropriately setting on-chip heaters. The photo insert shows the experimental configuration of E/O inputs and outputs (I/O) of our silicon chip. The modulated optical signal couples out of the chip and is amplified by a two stage EDFA to compensate for coupling loss. A programmable optical filter, a Finisar Waveshaper, is placed after the MZM for optical-domain precompensation before transmission. The digital and optical precompensation filters are jointly optimized to minimize BER, as discussed in the next section. Another tunable optical bandpass filter is deployed to reject out-of-band ASE noise.

Dual-polarization operation is achieved using a polarization division multiplexing emulator (PDME) implemented by separating polarization components and delaying one relative to the other. For experiments at longer distances, the signal is boosted before launching into the fiber transmission loop. The recirculation loop consists of an 80 km SMF, an EDFA and a Waveshaper; recirculation is controlled by two optical switches. The in-loop Waveshaper is programmed with a tilted passband to equalize the EDFA gain spectrum and reject the out-of-band ASE noise.

At the receiver, the transmitted signal is amplified to 6 dBm before coherent detection. To sweep OSNR in B2B operation, the signal is coupled with a power controlled 1-nm-wide ASE noise. The signal mixes with an 18 dBm local oscillator with a 100 kHz linewidth in a 2x8 optical hybrid. The hybrid products are O/E converted by four 70 GHz balanced detectors. The electrical signals are then captured by two synchronized RTO with 60 GHz analog bandwidth and a 160 GSa/s sampling rate.

National Science and Engineering Research Council of Canada (NSERC) Funding: CRDPJ 486716-15

The captured signal is recovered using offline DSP, as shown in the insert. We use fully blind DSP for signal processing. The captured signals are first filtered by a tenth order super-Gaussian low pass filter (LPF) with a bandwidth determined by the symbol rate. To minimize receiver-side skew-induced signal degradation,we adopt an independent I and Q branch equalization for chromatic dispersion compensation and adaptive multi-input-multi-output (MIMO) [19]. That is, after the LPF the four IQ tributaries are processed by four independent frequency-domain-implemented chromatic dispersion compensators (CDCs), and then are feed to a complex-valued 4-by-2 MIMO equalizer adapted using the constant modulus and multi-modulus techniques. After MIMO, the frequency offset is compensated using a fast Fourier transform (FFT)-based method, and the carrier phase is recovered using blind phase search. A 256-tap decision-directed least mean square (DD-LMS) filter is applied to further improve signal SNR. Finally, the recovered symbols are demodulated for BER calculation.

4. E/O optimization for high baud rate

For a depletion-mode SiP modulator, a key operating parameter is the DC bias voltage of the PN junction, which affects both V_π and modulator bandwidth. Higher DC bias increases the modulator bandwidth, but sacrifices V_π, lowering the OSNR due to a higher modulation loss for a fixed RF drive swing. This efficiency-bandwidth trade-off requires joint optimization of the modulator design and its bias to maximize the transmission performance [20]. Since high-baud-rate QAM requires more stringent OSNR, we use a relatively low reverse bias voltage of 0.75 V. This bias voltage results in a V_π of ~7.25 V, leading to a moderate modulation loss. The loss of the driving signal due to the limited modulator bandwidth is less than 10 dB in power at 40 GHz.

Due to our aggressive bit rate targets, the limited transmitter bandwidth requires the use of pre-compensation. The overall frequency response of our transmitter suffers more than 20 dB RF loss at frequency of 40 GHz (approximately ~10 dB from the DAC and ~10 dB from the modulator). As a result, a high baud rate signal would suffer from strong inter symbol interference (ISI). Digital pre-compensation (DPC) can be achieved without additional hardware complexity if a DAC is already employed for signal generation. However, it leads to reduced RF swing and extra modulation loss. In this system, full DPC would cause attenuation of more than 20 dB for some frequency content , resulting in excessive DAC quantization noise in driving signals.

The utse of optical pre-compensation (OPC) avoids quantization noise, but sees some signal content already suppressed by the transmitter. Splitting the pre-compensation across digital and optical may enable better performance [3]. This allows us to use just enough DPC to avoid the transmitter severely cutting off the signal to avoid significant reduction of the RF swing. We then rely on another pre-compensation stage (i.e., OPC) to provide additional signal conditioning to avoid ISI. However, independently designed digital and optical pre-compensation filters cannot guarantee the best trade-off between the quantization noise (from the DAC) and the SNR distribution across the signal frequency range (mostly degraded by ASE noise), especially in the presence of bandwidth limitation in high-baud-rate implementation. Therefore, we conduct a joint digital and optical optimization on the split of pre-compensation filters to maximize transmitter SNR.

The procedure to implement the digital and optical pre-compensation filters is illustrated in Fig. 3. There are roughly four stages. In the first stage we characterize our equipment. In the second stage we find the required total pre-compensation frequency response $H_{eff}(f)$. In the third stage we decompose this response into a smoothed part (destined for OPC in optical signal processing, OSP) and a residual rippled part (destined for DPC in DSP). The final stage seeks weighting factors for the OPC/DPC split.

In the measurement stage, we first characterize the DAC frequency response, $H_{DAC}(f)$, and develop a digital compensation by a DAC-to-RTO MMSE filter, i.e, $H_{DAC}^{-1}(f)$. With this

National Science and Engineering Research Council of Canada (NSERC) Funding: CRDPJ 486716-15

compensation in place, we use the high-resolution OSA to characterize the remaining frequency response to be compensated, $H_{OSA}(f)$. We load the DAC with a pre-compensated 84-Gbaud Nyquist-16QAM signal using the $H_{DAC}(f)$ found previously. We then capture the optical spectrum $H_{OSA}(f)$ using the OSA; assuming perfect DAC pre-compensation, it represents the signal bandwidth roll-off induced by driver and modulator.

The overall pre-compensation is

$$H_{eff}^{-1}(f) = H_{DAC}^{-1}(f)H_{OSA}^{-1}(f) \tag{1}$$

One measurement result is illustrated as the insert in Fig. 3 in the black curve. We use a polynomial equation fitting to obtain a smoothed curve $\tilde{H}_{eff}^{-1}(f)$, indicated by the pink dashed curve in the Fig. 3 inset. Using the fitted curve, we decompose the overall pre-compensation into this smooth part and a residual flat part with ripple. This decomposition allows us to assign to OPC only the smooth variation in frequency. The DPC will be responsible for the ripple.

We do not use a simple assignment of ripple to DPC and smooth to OPC. The ripple would not provide enough DPC to avoid severe filtering of the signal by the transmitter. Rather we distribute the smooth section across DPC and OPC using weighting factors α and β, respectively. The final pre-compensation is

$$H_{eff}^{-1}(f,\alpha,\beta) = \underbrace{\frac{H_{eff}^{-1}(f)}{\tilde{H}_{eff}^{-1}(f)}\left|\tilde{H}_{eff}^{-1}(f)\right|^{\alpha}}_{H_{DPC}^{-1}(f,\alpha)} \underbrace{\left|\tilde{H}_{eff}^{-1}(f)\right|^{\beta}}_{H_{OPC}^{-1}(f,\beta)} \tag{2}$$

Clearly, if $\alpha+\beta = 1$, the overall pre-compensation filter is $H_{eff}^{-1}(f)$ and we have full compensation; $\alpha+\beta < 1$ leads to under compensation, $\alpha+\beta > 1$ leads to over compensation, and $\alpha+\beta = 0$ causes only the ripple to be compensated in the digital domain. The blue and red curves in the Fig. 3 inset give an example decomposition into digital and optical domains, respectively.

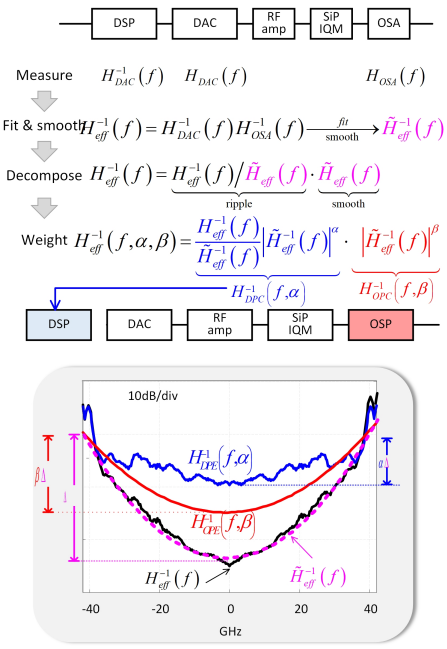

Fig. 3. Procedure to optimize split of pre-compensation between digital and optical domains.

National Science and Engineering Research Council of Canada (NSERC) Funding: CRDPJ 486716-15

For a more direct visual interpretation of the weighting parameters α and β, suppose the maximal excursion of $\tilde{H}_{eff}^{-1}(f)$ is denoted by Δ in dB, i.e. $\Delta = max(\log\left|\tilde{H}_{eff}^{-1}(f)\right|^2)$. This indicates the degree of pre-emphasis required; larger Δ implemented solely in the digital domain would lead to severe restriction of RF voltage swing. The new depth of the DPC is $\alpha\Delta$, and this is the number we use to parameterize the DPC. In the optical domain the parameterization is $\beta\Delta$.

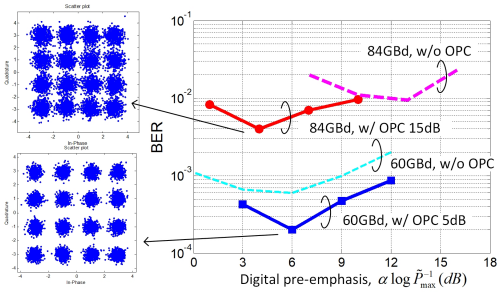

Fig. 4. Optimization of pre-compensation filters for 60 Gbaud and 84 Gbaud 16QAM.

The optimization of pre-compensation filters is carried out by running 16QAM single polarization signals in an optical B2B system and measuring the BER for various values of $\alpha\Delta$ and $\beta\Delta$. Figure 4 sweeps $\alpha\Delta$ for fixed values of $\beta\Delta$. We consider both 60 Gbaud (~34 dB OSNR) and 84 Gbaud (~29 dB OSNR) transmissions; optimization will vary with baud rate. The dashed lines in Fig. 4 show the BER dependence on $\alpha\Delta$ for digital pre-compensation alone (i.e. $\beta = 0$). Solid lines with markers are results with optimal optical pre-compensation filters at the same baud rates. As can be seen, OPC leads to low BER, and the optimal $\alpha\Delta$ shifts. A two dimensional optimization was performed, but only the best $\beta\Delta$ curve is presented.

For 60 Gbaud 16QAM, the lowest BER can be improved from 6e-4 (Q^2 = 10.2 dB) to 2e-4 (Q^2 = 11 dB) (about 0.8 dB improvement in Q^2 factor) when setting 10 dB DPC ($\alpha\Delta$ = 10 dB) combined with 5 dB OPC ($\beta\Delta$ = 5 dB). For 84 Gbaud 16QAM, the best BER of ~4e-3 (Q^2 = 8.5 dB) is obtained by 8 dB DPC and 15 dB OPC; in contrast, only 1e-2 (Q^2 = 7.4 dB) could be achieved with DPC alone, indicating about 1dB Q^2 factor improvement by joint OPC-DPC optimization. The best achieved constellations at each baud rate are also illustrated in Fig. 4. It worth mentioning that the optical pre-compensation can be implemented using passive optical components on the same chip [12]. In experiments reported in the next sections, combined OPC and DPC are used. In addition to values reported in Fig. 4, for 72 Gbaud we use 11 dB DPC and 6 dB OPC, and for 75 Gbaud we have 12 dB DPC and 7 dB OPC.

5. Results and discussion

5.1. Back-to-back performance

Figure 5 shows the BER versus OSNR curves of 16/32 QAM with various baud rates. These data formats allow single carrier transmission tests with raw bit rates ranging from 480 Gb/s to 720 Gb/s. We evaluate the system performance using pre-FEC BER thresholds, assuming 7% FEC overhead of 3.8e-3 [21] and 20% FEC of 2.4e-2 [22]. With 16QAM modulation format, the required OSNR values for 60/75 Gbaud to reach the 7% FEC threshold are 25.5 dB and 28.5 dB, respectively. In the case of 20% FEC, the required OSNR for 60 and 75 Gbaud 16QAM are 22 dB and 23 dB, indicating a penalty of 2.7 dB and 3.3 dB, respectively, compared to the theoretical BER curves. When transmitting at 84 Gbaud, the required OSNR for 20% FEC is 25 dB, and 4.3 dB OSNR penalty compared to theory. With 32QAM modulation format, 60 Gbaud signals can barely reach the 7% FEC threshold even at the highest OSNR of ~33 dB. For 72 Gbaud, the

National Science and Engineering Research Council of Canada (NSERC) Funding: CRDPJ 486716-15

highest OSNR we can achieve is less than 32 dB, and it gives a BER slightly lower than 2e-2; for 20% FEC we need 29.5 dB. The observed OSNR penalties for implementing 32QAMs are 2.9 dB and 5.5 dB for 60 Gbaud and 72 Gbaud, respectively. The OSNR penalty increases when running at higher baud rates and higher modulation formats, which are mostly caused by the degraded performance (SNR and the effective number of bits) of the DAC in the high-frequency range.

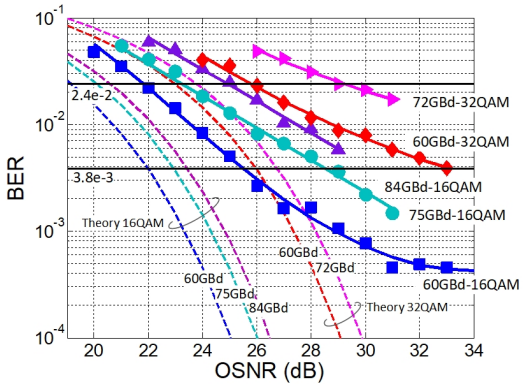

Fig. 5. BER v.s. OSNR curves for 60/75/84 Gbaud 16QAM and 60/72 Gbaud 32QAM. The dashed lines are the theoretical prediction for an ideal transceiver system. The solid lines are the experimental results.

These BER curves reveal that the major performance limitation is the limited OSNR that can be achieved when using a SiP modulator. In tests above 60 Gbaud the BER curves are linear; OSNR is not sufficient to reach ISI-induced BER floors. Only 60 Gbaud 16QAM transmissions indicate a BER floor for OSNR above 31 dB. In our test, the OSNR degradation is mainly incurred by transmitter loss. One of the losses comes from optical I/O coupling of the SiP chip, which is ~4.3 dB per GC, as previously mentioned. This value is expected to be lower when using edge coupling. Another major source of loss is modulation loss, which relates to the modulation depth denoted by driving swing over V_π. Smaller swing and larger V_π will lead to greater modulation loss. In our test, the RF driving swing (after applying digital precompensation) decreases from ~3.5 V_{pp} at 60 Gbaud to ~1.4 V_{pp} at 84 Gbaud. Moreover, the V_π of our SiP IQM is around 7 V, which is high compared to other semiconductor or $LiNbO_3$ modulators. All these factors limit the highest achievable OSNR for seeding the chip.The OSNR can be significantly improved with a lower input laser power using low-loss optical IOs for which recent progress has shown a broadband coupling efficiency of greater than -1 dB. [23]

5.2. Transmission results

The launch power is optimized first by probing a 60 Gbaud 16QAM with different powers at 560 km transmission. Figure 6(a) shows the BER and launch power dependence. A 2 dBm launch power provides the best BER performance for the single carrier dual-polarization signal. The balance of transmission tests reported use a 2 dBm launch power.

The BER results for distance transmissions are summarized in Fig. 6(b). For 60 Gbaud 16QAM, blue curve with square marker, a raw data rate of 480 Gb/s can span about 1,520 km with BER lower than the FEC threshold, roughly providing a net 400 Gb/s after accounting for the FEC overhead. The 500 Gb/s (raw 600 Gb/s) test configuration is realized by 75 Gbaud 16QAM and 60 Gbaud 32QAM, as indicated by the light blue curve with round markers and the red curve with diamond markers, respectively. The net 500 Gb/s signal can span approximately 1,120 km with 75 Gbaud 16QAM, or a shorter distance of about 480 km with higher spectral

National Science and Engineering Research Council of Canada (NSERC) Funding: CRDPJ 486716-15

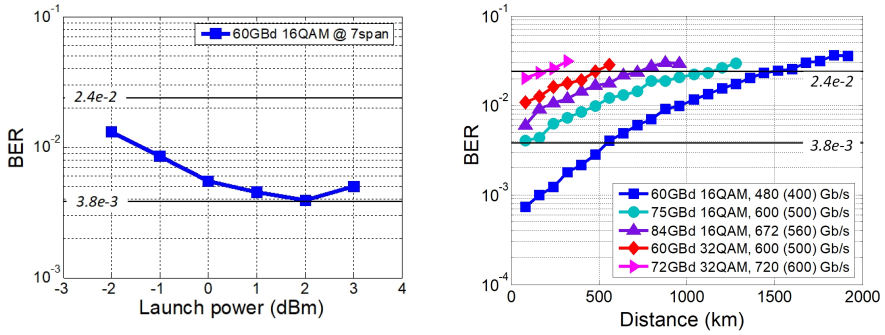

(a) (b)

Fig. 6. (a) BER of 60 Gbaud 16QAM for different launch power at 560 km transmission; (b) BER for 60/75/84 Gbaud 16QAM and 60/72 Gbaud 32QAM for swept transmission distance. Raw bit rates are reported in the legend, as well as post-FEC-overhead bit rates in parentheses.

efficiency with 32QAM. The 84 Gbaud 16QAM (purple curve with up-triangle marker) provides a raw bit rate of 672 Gb/s, the achieved distance is about 720 km with 20% FEC, resulting in a net bit rate of 560 Gb/s. The highest bit rate is achieved by 72 Gbaud 32QAM (pink curve with right-triangle marker), which provides 720 Gb/s raw bit rate. Assuming the use of a 20% FEC, the raw 720 Gb/s signal can span about 160 km, resulting a net rate of ~600 Gb/s.

6. Conclusion

We have realized high-baud-rate QAM generation and transmission using a CMOS-compatible silicon IQ modulator. We have demonstrated a joint optimization procedure of optical and digital pre-emphasis filters, and applied it to the silicon coherent transmitter. Single carrier transmission with post-FEC-overhead bit rates spanning 400 Gb/s to 600 Gb/s have been demonstrated over hundreds of kilometers. Using moderate complexity 7% overhead FEC, over 500 km have been achieved at 400 Gb/s, the target of the 400GbE Ethernet standard. Using a more aggressive FEC (20% in our case), rates as high as 600 Gb/s have been achieved even in our SNR-limited demonstration. These results demonstrate the efficacy of all-silicon modulators in achieving higher-order modulation formats for ultra-high-capacity coherent optical communications systems. The advantages of SiP integration can be reaped even at these extreme bit rates.

Funding

Huawei Canada; Natural Sciences and Engineering Research Council of Canada (CRDPJ 486716-15).

Acknowledgments

The authors thank Dr. Zhuhong Zhang and his team with Huawei Canada for many useful discussions. The authors also thank Nelson Landry for his technical support and CMC Microsystems for the fabrication subsidy and MPW service.

References

1. J. Zhang, J. Yu, B. Zhu, and H.-C. Chien, "WDM transmission of single-carrier 120-GBd ETDM PDM-16QAM signals over 1200-km terrestrial fiber links," J. Light. Technol. **35**, 1033–1040 (2017).

2. G. Raybon, A. Adamiecki, J. Cho, P. Winzer, A. Konczykowska, F. Jorge, J. Dupuy, M. Riet, B. Duval, K. Kim, S. Randel, D. Pilori, B. Guan, N. Fontaine, and E. C. Burrows,"Single-carrier all-ETDM 1.08-Terabit/s line rate PDM-64-QAM transmitter using a high-speed 3-bit multiplexing DAC," in *IEEE Photonics Conference* (IEEE, 2015), pp. 1–2.
3. K. Schuh, F. Buchali, W. Idler, T. A. Eriksson, L. Schmalen, W. Templ, L. Altenhain, U. Dümler, R. Schmid, M. Möller, and Klaus Engenhardt, "Single carrier 1.2 Tbit/s transmission over 300 km with PM-64 QAM at 100 GBaud," in *Optical Fiber Communications Conference and Exhibition (OFC)* (IEEE, 2017), pp. 1–3.
4. V. Lal, J. Summers, N. Kim, S. W. Corzine, P. Evans, M. Lauermann, A. Nguyen, A. Hosseini, M. Lu, J. T. Rahn, M. R. Chitgarha, J. Zhang, J. Osenbach, T. Vallaitis, P. Samra, C. Park, M. Kuntz, J. Tang, C. Tsai, H. Sun, R. Schmogrow, D. Pavinski, B. Behnia, P. Mertz, T. Butrie, K.-T. Wu, M. Mitchell, M. Ziari, M. Reffle, D. Welch, and F. Kish, "Extended C-band tunable multi-channel InP-based coherent transmitter PICs," J. Light. Technol. **35**, 1320–1327 (2017).
5. R. Going, M. Lauermann, R. Maher, H. Tsai, M. Lu, N. Kim, S. Corzine, P. Studenkov, J. Summers, A. Hosseini, J. Zhang, B. Behnia, J. Tang, S. Buggaveeti, T. Vallaitis, J. Osenbach, M. Kuntz, X. Xu, K. Croussore, V. Lal, P. Evans, J. Rahn, T. Butrie, A. Karanicolas, K.-T. Wu, M. Mitchell, M. Ziari, D. Welch, and F. Kish, "Multi-channel InP-based coherent PICs with hybrid integrated SiGe electronics operating up to 100 GBd 32QAM," in *European Conference on Optical Communication (ECOC)* (IEEE, 2017), pp. 1-3.
6. M. Y. Sowailem, T. M. Hoang, M. Morsy-Osman, M. Chagnon, M. Qiu, S. Paquet, C. Paquet, I. Woods, Q. Zhuge, O. Liboiron-Ladouceur, and D. V. Plant, "770-Gb/s PDM-32QAM coherent transmission using InP dual polarization IQ modulator," IEEE Photonics Technol. Lett. **29**, 442–445 (2017).
7. Y. Ogiso, J. Ozaki, Y. Ueda, N. Kashio, N. Kikuchi, E. Yamada, H. Tanobe, S. Kanazawa, H. Yamazaki, Y. Ohiso, T. Fujii, and M. Kohtoku, "Over 67 GHz bandwidth and 1.5 V Vπ InP-based optical IQ modulator with n-i-p-n heterostructure," J. Light. Technol. **35**, 1450–1455 (2017).
8. G. Raybon, J. Cho, A. Adamiecki, P. Winzer, L. Carvalho, J. Oliveira, A. Konczykowska, J.-Y. Dupuy, and F. Jorge, "180-Gb/s (90-GBd QPSK) single carrier transmitter using a thin film polymer on silicon I/Q modulator," in *ECOC 2016; 42nd European Conference on Optical Communication* (IEEE, 2016), pp. 1–3.
9. S. Wolf, H. Zwickel, C. Kieninger, M. Lauermann, W. Hartmann, Y. Kutuvantavida, W. Freude, S. Randel, and C. Koos, "Coherent modulation up to 100 GBd 16QAM using silicon-organic hybrid (SOH) devices," Opt. Express **26**, 220–232 (2018).
10. M. Hochberg, N. C. Harris, R. Ding, Y. Zhang, A. Novack, Z. Xuan, and T. Baehr-Jones, "Silicon photonics: the next fabless semiconductor industry," IEEE Solid-State Circuits Mag. **5**, 48–58 (2013).
11. J. S. Orcutt, B. Moss, C. Sun, J. Leu, M. Georgas, J. Shainline, E. Zgraggen, H. Li, J. Sun, M. Weaver, S. Urošević, M. Popović, R. J. Ram, and V. Stojanović, "Open foundry platform for high-performance electronic-photonic integration," Opt. Express **20**, 12222–12232 (2012).
12. P. Dong, C. Xie, L. L. Buhl, Y.-K. Chen, J. H. Sinsky, and G. Raybon, "Silicon in-phase/quadrature modulator with on-chip optical equalizer," J. Light. Technol. **33**, 1191–1196 (2015).
13. J. Geyer, C. Doerr, M. Aydinlik, N. Nadarajah, A. Caballero, C. Rasmussen, and B. Mikkelsen, "Practical implementation of higher order modulation beyond 16-QAM," in *Optical Fiber Communications Conference and Exhibition (OFC)* (IEEE, 2015), pp. 1–3.
14. C. Y. Wong, S. Zhang, Y. Fang, L. Liu, T. Wang, Q. Zhang, S. Deng, G. N. Liu, and X. Xu, "Silicon IQ modulator for next-generation metro network," J. Light. Technol. **34**, 730–736 (2016).
15. X. Xiao, M. Li, L. Wang, D. Chen, Q. Yang, and S. Yu, "High speed silicon photonic modulators," in *Optical Fiber Communications Conference and Exhibition (OFC)* (IEEE, 2017), pp. 1–3.
16. P. Dong, L. Chen, and Y.-k. Chen, "High-speed low-voltage single-drive push-pull silicon Mach-Zehnder modulators," Opt. Express **20**, 6163–6169 (2012).
17. H. Bahrami, H. Sepehrian, C. S. Park, L. A. Rusch, and W. Shi, "Time-domain large-signal modeling of traveling-wave modulators on SOI," J. Light. Technol. **34**, 2812–2823 (2016).
18. L. Jiang, X. Chen, K. Kim, G. de Valicourt, Z. R. Huang, and P. Dong, "Electro-optic crosstalk in parallel silicon photonic Mach-Zehnder modulators," J. Light. Technol. **36**, 1713–1720 (2018).
19. R. Rios-Müller, J. Renaudier, and G. Charlet, "Blind receiver skew compensation and estimation for long-haul non-dispersion managed systems using adaptive equalizer," J. Light. Technol. **33**, 1315–1318 (2015).
20. H. Sepehrian, A. Yekani, W. Shi, and L. A. Rusch, "Assessing performance of silicon photonic modulators for pulse amplitude modulation," IEEE J. Sel. Top. Quantum Electron. **24**, 1–10 (2018).
21. International Telecommunication Union, *Recommendation G.975.1, Appendix I.9* (2004).
22. D. Chang, F. Yu, Z. Xiao, Y. Li, N. Stojanovic, C. Xie, X. Shi, X. Xu, and Q. Xiong, "FPGA verification of a single QC-LDPC code for 100 Gb/s optical systems without error floor down to BER of 10-15," in *Optical Fiber Communication Conference and Exhibition and the National Fiber Optic Engineers Conference* (IEEE, 2011), pp. 1–3.
23. L. Jia, C. Li, T.-Y. Liow, and G. Q. Lo, "Efficient suspended coupler with loss less than- 1.4 db between si-photonic waveguide and cleaved single mode fiber," J. Light. Technol. **36**, 239–244 (2018).

National Science and Engineering Research Council of Canada (NSERC) Funding: CRDPJ 486716-15